PHYSICAL REVIEW D **91,** 054024 (2015)

Single- and central-diffractive production of open charm and bottom mesons at the LHC: Theoretical predictions and experimental capabilities

Marta Łuszczak[*]
University of Rzeszów, PL-35-959 Rzeszów, Poland

Rafał Maciuła[†] and Antoni Szczurek[‡]
Institute of Nuclear Physics PAN, PL-31-342 Kraków, Poland
(Received 29 December 2014; published 20 March 2015)

We discuss diffractive production of open charm and bottom mesons at the LHC. The differential cross sections for single- and central-diffractive mechanisms for $c\bar{c}$ and $b\bar{b}$ pair production are calculated in the framework of the Ingelman-Schlein model corrected for absorption effects. In this approach, one assumes that the Pomeron has a well-defined partonic structure, and that the hard process takes place in a Pomeron-proton or proton-Pomeron (single diffraction) or Pomeron-Pomeron (central diffraction) process. Here, leading-order gluon-gluon fusion and quark-antiquark annihilation partonic subprocesses are taken into consideration, which are calculated within standard collinear approximation. Both Pomeron flux factors as well as parton distributions in the Pomeron are taken from the H1 Collaboration analysis of diffractive structure function and diffractive dijets at HERA. The extra corrections from subleading Reggeon exchanges are explicitly calculated and are also taken into consideration. Several quark-level differential distributions are shown. The hadronization of charm and bottom quarks is taken into account by means of fragmentation function technique. Predictions for single- and central-diffractive production in the case of inclusive D and B mesons, as well as $D\bar{D}$ pairs, are presented, including detector acceptance of the ATLAS, CMS, and LHCb collaborations. The experimental aspects of possible standard and dedicated measurements are carefully discussed.

DOI: 10.1103/PhysRevD.91.054024 PACS numbers: 13.87.Ce, 14.65.Dw

I. INTRODUCTION

Diffractive processes were intensively studied at HERA in γp and ep collisions for more than a decade. On the theoretical side, somewhat enigmatically, these are processes with the exchange of Pomerons or processes with the QCD amplitude without net color exchange. In such processes, Pomerons must be treated rather technically, depending on the formulation of the approach. Experimentally, such processes are defined by special requirements on the final state. The most popular is the requirement of a rapidity gap starting from the final proton(s) on one (single-diffractive process) or both (central-diffractive process) sides. The size of the gap is essentially experimentally observable, but it is not easy to calculate theoretically. Several processes with different final states were studied at HERA, such as dijet, charm production, etc. The H1 Collaboration has found a set of so-called diffractive parton distributions in the proton inspired by the Ingelman-Schlein model [1]. In this fit, both Pomeron and Reggeon contributions were included. We wish to emphasize that there is no common consensus as far as a model of diffractive production is considered. However, these open problems go beyond the scope of the present paper and will be not discussed here.

One can gain a better understanding of the mechanism of the diffractive production by going from photon-proton to proton-proton or proton-antiproton scattering. There, however, some new elements related to nonperturbative interaction between protons show up, such as absorption effects. So far, only some selected diffractive processes have been discussed in the literature, such as diffractive production of dijets [2], production of W [3] and Z [4] bosons, production of W^+W^- pairs [5], or production of $c\bar{c}$ [6]. The latter was done there only for illustration of the general situation at the parton level. The cross sections for diffractive processes are in general rather small (e.g., the single-diffractive processes are of the order of a few percent compared to inclusive cross sections). In order to measure rapidity gap(s), the luminosity cannot be big, in order to avoid so-called pileups [7]. All of this means that for some interesting processes, such as, for instance, W or Z^0 production, the statistics is rather poor and the cross section is difficult to measure. Since the cross section for inclusive production of charm is very large at the LHC [8], one could expect that single- and central-diffractive charm production could also be measured with relatively good precision. This is therefore a process one could use for testing theoretical models. The same shall be true for diffractive bottom production.

[*]luszczak@univ.rzeszow.pl
[†]rafal.maciula@ifj.edu.pl
[‡]Also at University of Rzeszów, PL-35-959 Rzeszów, Poland. antoni.szczurek@ifj.edu.pl

It is the aim of this paper to present predictions including our knowledge about diffractive parton distributions from HERA and taking into account absorption effects, specific for proton-proton collisions. We shall include both Pomeron and Reggeon contributions. In addition, we shall include hadronization of c and b quarks/antiquarks to open charmed and bottom mesons, respectively. Finally, we shall present our predictions for experiments at the LHC. We hope that our predictions will be verified at the LHC in the near future.

II. THEORETICAL FRAMEWORK

A. A sketch of formalism

The mechanisms of the diffractive production of heavy quarks ($c\bar{c}$, $b\bar{b}$) discussed here are shown in Figs. 1 and 2. Both leading-order (LO) gg-fusion and $q\bar{q}$-anihilation partonic subprocesses are taken into account in the calculations.

In the following, we apply the Ingelman-Schlein approach [1]. In this approach, one assumes that the Pomeron has a well-defined partonic structure, and that the hard process takes place in a Pomeron-proton or proton-Pomeron (single diffraction) or Pomeron-Pomeron (central diffraction) process. In this approach, corresponding differential cross sections in rapidity of the quark y_1, rapidity of the antiquark y_2, and transverse momentum p_t of either of them can be written as

$$\frac{d\sigma_{\mathrm{SD}^{(1)}}}{dy_1 dy_2 dp_t^2} = \frac{1}{16\pi^2 \hat{s}^2} \times [|\mathcal{M}_{gg\to Q\bar{Q}}|^2 \cdot x_1 g^D(x_1,\mu^2) x_2 g(x_2,\mu^2) + |\mathcal{M}_{q\bar{q}\to Q\bar{Q}}|^2 \cdot (x_1 q^D(x_1,\mu^2) x_2 \bar{q}(x_2,\mu^2) + x_1 \bar{q}^D(x_1,\mu^2) x_2 q(x_2,\mu^2))], \tag{2.1}$$

$$\frac{d\sigma_{\mathrm{SD}^{(2)}}}{dy_1 dy_2 dp_t^2} = \frac{1}{16\pi^2 \hat{s}^2} \times [|\mathcal{M}_{gg\to Q\bar{Q}}|^2 \cdot x_1 g(x_1,\mu^2) x_2 g^D(x_2,\mu^2) + |\mathcal{M}_{q\bar{q}\to Q\bar{Q}}|^2 \cdot (x_1 q(x_1,\mu^2) x_2 \bar{q}^D(x_2,\mu^2) + x_1 \bar{q}(x_1,\mu^2) x_2 q^D(x_2,\mu^2))], \tag{2.2}$$

$$\frac{d\sigma_{\mathrm{CD}}}{dy_1 dy_2 dp_t^2} = \frac{1}{16\pi^2 \hat{s}^2} \times [|\mathcal{M}_{gg\to Q\bar{Q}}|^2 \cdot x_1 g^D(x_1,\mu^2) x_2 g^D(x_2,\mu^2) + |\mathcal{M}_{q\bar{q}\to Q\bar{Q}}|^2 \cdot (x_1 q^D(x_1,\mu^2) x_2 \bar{q}^D(x_2,\mu^2) + x_1 \bar{q}^D(x_1,\mu^2) x_2 q^D(x_2,\mu^2))], \tag{2.3}$$

for single-diffractive (SD) and central-diffractive (CD) production, respectively. Above, $\mathcal{M}_{gg\to Q\bar{Q}}$ and $\mathcal{M}_{q\bar{q}\to Q\bar{Q}}$ are on-shell matrix elements for considered hard partonic subprocesses, $g(x,\mu^2)$ and $q(x,\mu^2)$ are standard collinear gluon and quark (or antiquark) distribution functions (PDFs), and $g^D(x,\mu^2)$, $q^D(x,\mu^2)$ are their diffractive counterparts. The variables x_1 and x_2 are the parton longitudinal momentum fractions in the first or the second proton and $\hat{s} = x_1 x_2 s$.

The diffractive distribution function (diffractive PDF) can be obtained by a convolution of the flux of Pomerons $f_{\mathbf{IP}}(x_{\mathbf{IP}})$ in the proton and the parton distribution in the Pomeron, e.g., $g_{\mathbf{IP}}(\beta,\mu^2)$ for gluons:

$$g^D(x,\mu^2) = \int dx_{\mathbf{IP}} d\beta \delta(x - x_{\mathbf{IP}}\beta) g_{\mathbf{IP}}(\beta,\mu^2) f_{\mathbf{IP}}(x_{\mathbf{IP}}) = \int_x^1 \frac{dx_{\mathbf{IP}}}{x_{\mathbf{IP}}} f_{\mathbf{IP}}(x_{\mathbf{IP}}) g_{\mathbf{IP}}\left(\frac{x}{x_{\mathbf{IP}}},\mu^2\right). \tag{2.4}$$

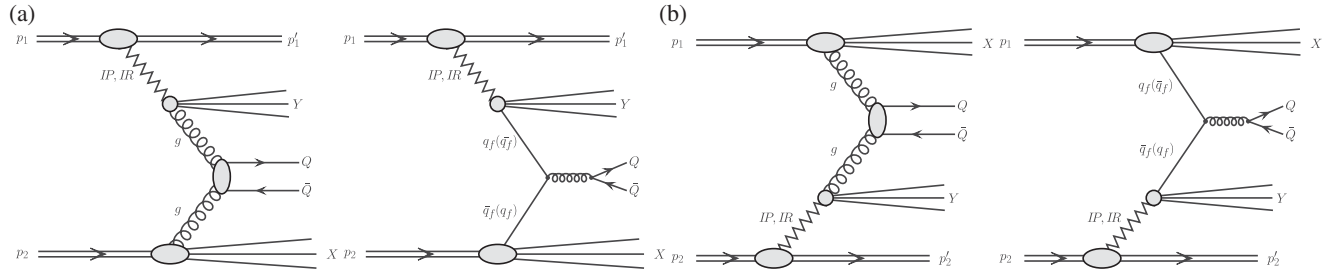

FIG. 1. The mechanisms of single-diffractive production of heavy quarks in the case of Pomeron-parton (a) or parton-Pomeron (b) interactions.

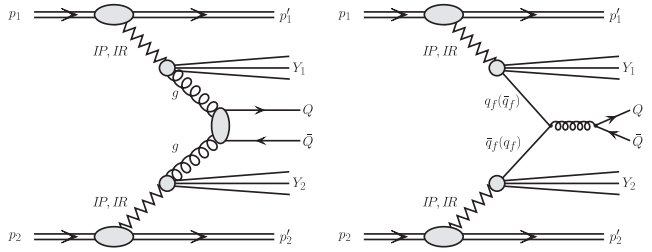

FIG. 2. The mechanisms of central-diffractive production of heavy quarks.

The flux of Pomerons $f_{\mathbf{IP}}(x_{\mathbf{IP}})$ enters in the form integrated over four-momentum transfer

$$f_{\mathbf{IP}}(x_{\mathbf{IP}}) = \int_{t_{\min}}^{t_{\max}} dt f(x_{\mathbf{IP}}, t), \tag{2.5}$$

with $t_{\min}, t_{\max}$ being kinematic boundaries.

Both Pomeron flux factors $f_{\mathbf{IP}}(x_{\mathbf{IP}}, t)$ as well as parton distributions in the Pomeron were taken from the H1 Collaboration analysis of diffractive structure function and diffractive dijets at HERA [9]. In the following calculation, standard collinear MSTW08LO parton distributions are used [10]. The renormalization scale in α_s and factorization scale for the diffractive PDFs are taken to be equal to heavy (charm or bottom) quark transverse mass $\mu = m_t$ (should not be mixed with top quark mass) as a default and $\mu = \hat{s}$ for illustration of related uncertainty. The heavy quark mass in the calculation is set to 1.5 and 4.75 GeV for charm and bottom, respectively.

B. Results for diffractive $Q\bar{Q}$ pair production

Let us start the presentation of our results for diffraction mechanisms. In the present analysis, we consider both Pomeron and subleading Reggeon contributions. In the H1 Collaboration analysis, the pion structure function was used for the subleading Reggeons, and the corresponding flux was fitted to the diffractive DIS data. The corresponding diffractive parton distributions are obtained by replacing the Pomeron flux with the Reggeon flux, and the parton distributions in the Pomeron with their counterparts in the subleading Reggeon [9].

In Fig. 3 we show the transverse momentum distribution of c quarks (antiquarks) and b quarks (antiquarks) for single-diffractive production at $\sqrt{s} = 14$ TeV. Contributions of the Pomeron-gluon (and gluon-Pomeron), the Pomeron-quark/antiquark (and quark/antiquark-Pomeron), the Reggeon-gluon (and gluon-Reggeon), and the Reggeon-quark/antiquark (and quark/antiquark-Reggeon) mechanisms are shown separately. The components of the Pomeron-gluon (and gluon-Pomeron) are almost 2 orders of magnitude larger than those of the Pomeron-quark/antiquark and quark/antiquark-Pomeron. The estimated Reggeon contribution is of similar size to the leading Pomeron contribution, but still slightly smaller.

For the considered reaction, the corresponding Reggeon contribution is rather small, and therefore it cannot be extracted by studying experimental data. However, in the measurement of leading protons at HERA it is better visible and seems necessary to describe the experimental data [11–13]. The isoscalar Reggeon exchange is absolutely necessary in the description of the total cross section for pp, $p\bar{p}$, πp, and corresponding elastic scatterings [14]. In our recent analysis of the $pp \to pp\pi^+\pi^-$ reaction, the presence of the isoscalar Reggeon exchange is also very important, and the strength of the contribution is consistent with that obtained from the analysis of total and elastic cross sections [15].

The calculation done assumes Regge factorization, which is known to be violated in hadron-hadron collisions.

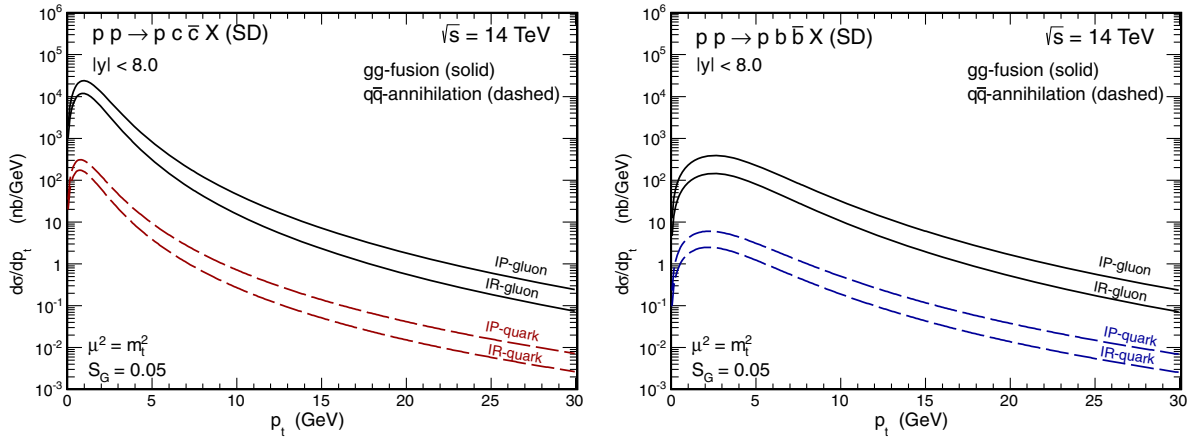

FIG. 3 (color online). Transverse momentum distribution of c quarks (antiquarks) (left) and b quarks (antiquarks) (right) for single-diffractive production at $\sqrt{s} = 14$ TeV. Components of the Pomeron-gluon (and gluon-Pomeron), the Pomeron-quark/antiquark (and quark/antiquark-Pomeron), the Reggeon-gluon (and gluon-Reggeon), and the Reggeon-quark/antiquark (and quark/antiquark-Reggeon) mechanisms are shown separately.

It is known that soft interactions lead to an extra production of particles which fill in the rapidity gaps related to Pomeron exchange.

Different models of absorption corrections (one-, two- or three-channel approaches) for diffractive processes were presented in the literature. The absorption effects for the diffractive processes were calculated, e.g., in Refs. [4,16,17]. The different models give slightly different predictions. Usually an average value of the gap survival probability $\langle |S_G|^2 \rangle$ is calculated first, and then the cross sections for different processes are multiplied by this value. We shall follow this somewhat simplified approach also here. Numerical values of the gap survival probability can be found in Refs. [4,16,17]. The survival probability depends on the collision energy. It is sometimes parametrized as

$$\langle S_G^2 \rangle(\sqrt{s}) = \frac{a}{b + \ln(\sqrt{s})}. \tag{2.6}$$

The multiplicative factors are approximately $S_G = 0.05$ for single-diffractive production and $S_G = 0.02$ for central-diffractive production for the nominal LHC energy ($\sqrt{s} = 14$ TeV).

We have checked in purely exclusive (e.g., $pp \to ppJ/\psi$ [18], $pp \to pp\pi^+\pi^-$ [15]) reactions that the crucial variables for absorptive corrections are four-momentum transfers squared (t_1 or t_2) in proton lines. The t dependence for Pomeron and Reggeon exchange is phenomenologically rather similar (similar slope parameter), so the resulting gap survival factor should also be similar. Taking into account all other uncertainties discussed partially in our paper, such an approximation should therefore be sufficient.

In Fig. 4 we show the transverse momentum distribution of c quarks (antiquarks) and b quarks (antiquarks) for central-diffractive production at $\sqrt{s} = 14$ TeV. The distribution for the central-diffractive component is smaller than that for the single-diffractive distribution by almost 2 orders of magnitude.

In Fig. 5 we show separately contributions for different upper limits for the values of $x_{\mathbf{IP}}$ and $x_{\mathbf{IR}}$. The shapes of these distributions are rather similar. As a default, in the case of Pomeron exchange, the upper limit in the convolution formula is taken to be 0.1, and for Reggeon exchange it is 0.2. Additionally, Fig. 6 shows the distribution in Pomeron/Reggeon longitudinal momentum fraction for c quarks (antiquarks) (left panel) and for b quarks (antiquarks) (right panel) for single-diffractive production. The similar distributions in $\log_{10} x_{\mathbf{IP}}$ and $\log_{10} x_{\mathbf{IR}}$ are presented in Fig. 7. In our opinion, the whole Regge formalism does not apply above these limits, and therefore unphysical results could be obtained. The simple formula for the Pomeron flux was never tested/checked experimentally beyond the Pomeron longitudinal momentum fraction equaling 0.1. This is known, for instance, from the studies of leading protons at HERA [11]. There, for instance, the subleading isoscalar Reggeon contribution starts to be bigger than the Pomeron contribution and has to be taken into account. If we were still to increase the longitudinal momentum fraction, we would also have to take into account neutral pion exchange. However, for neutral pion exchange, the corresponding rapidity gap is smaller, and a full simulation of the final state would be necessary. Therefore, it is a compromise that we take the upper Reggeon longitudinal momentum fraction as big as 0.2. In practice in the LHC experiments, due to beam optics, one can measure proton longitudinal momentum fractions down to about 0.85—that is, the corresponding upper limit for the Pomeron/Reggeon momentum fraction is about 0.15.

For completeness, in Fig. 8 we show separately contributions for different factorization scales: $\mu^2 = m_t^2$ and $\mu^2 = \hat{s}$, which give quite similar distributions in transverse momentum.

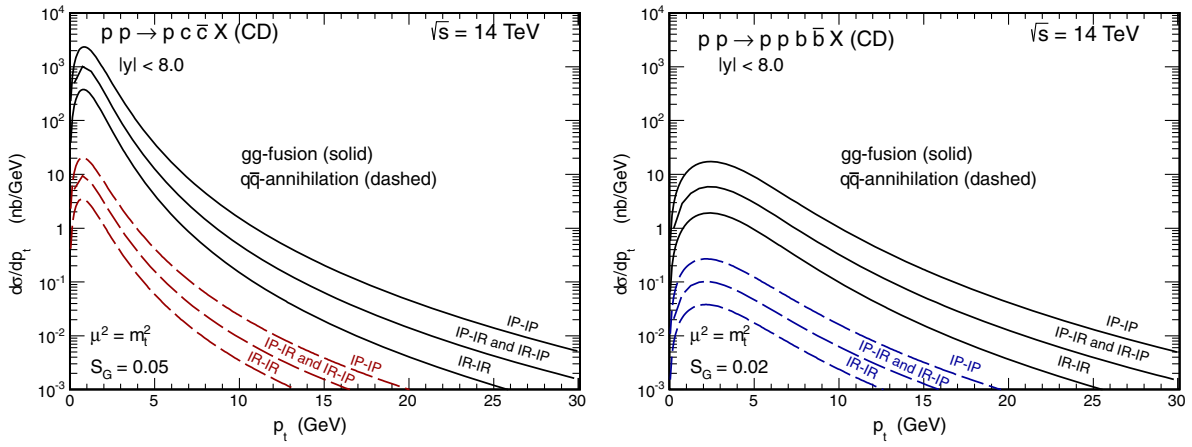

FIG. 4 (color online). Transverse momentum distribution of c quarks (antiquarks) (left) and b quarks (antiquarks) (right) for the central-diffractive production at $\sqrt{s} = 14$ TeV. Components of the Pomeron-Pomeron, Reggeon-Reggeon, Pomeron-Reggeon, and Reggeon-Pomeron mechanisms are shown separately.

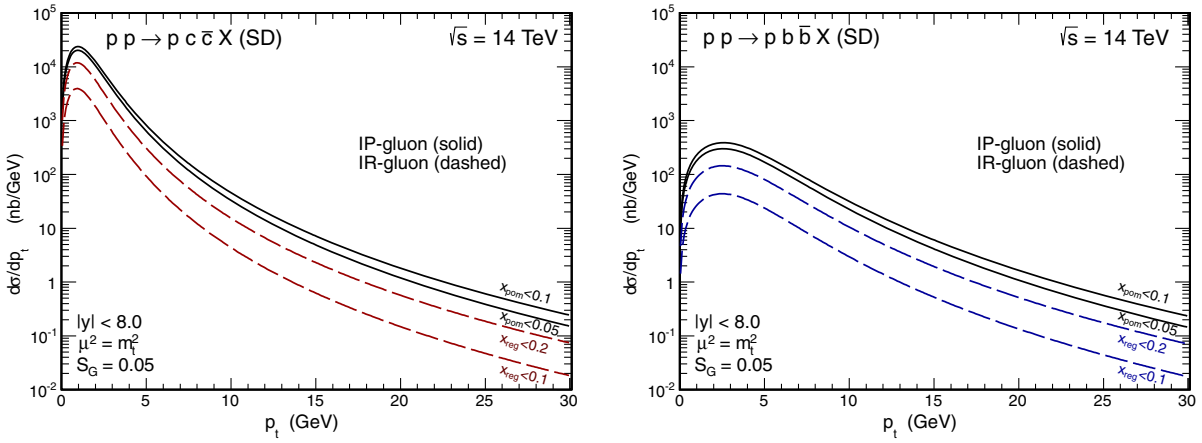

FIG. 5 (color online). Transverse momentum distribution of c quarks (antiquarks) (left) and b quarks (antiquarks) (right) for single-diffractive production at $\sqrt{s} = 14$ TeV for different maximal $x_{\mathbf{IP}}$ (solid) and $x_{\mathbf{IR}}$ (dashed).

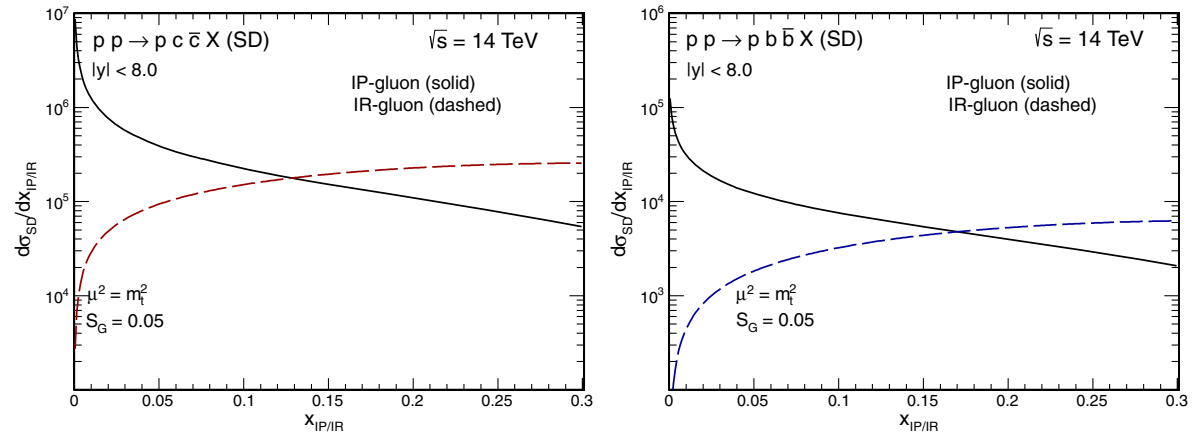

FIG. 6 (color online). The distribution in $x_{\mathbf{IP}}$ (solid) and $x_{\mathbf{IR}}$ (dashed) for $\sqrt{s} = 14$ TeV. The left panel shows distribution in Pomeron/Reggeon longitudinal momentum fraction for c quarks (antiquarks); the right panel shows similar distributions for b quarks (antiquarks) for single-diffractive production.

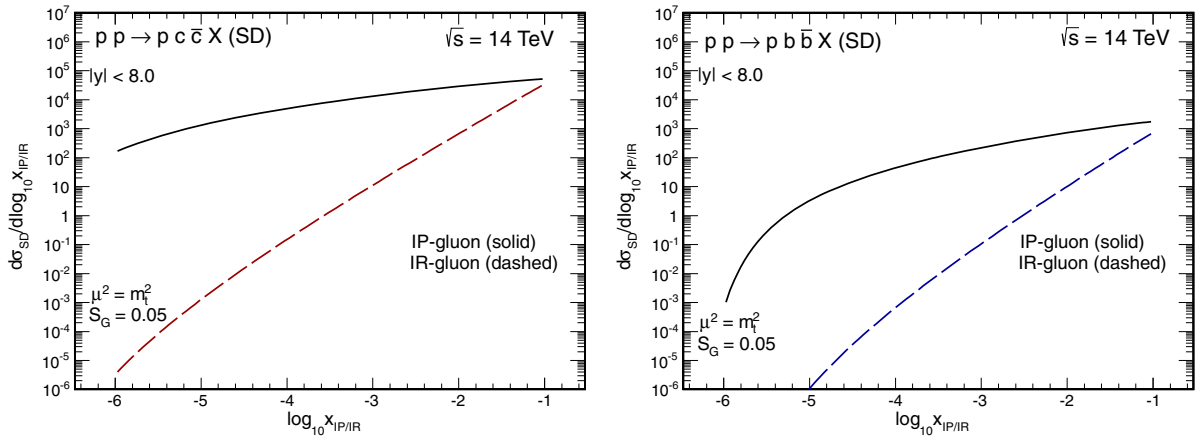

FIG. 7 (color online). The distribution in $\log_{10} x_{\mathbf{IP}}$ (solid) and $\log_{10} x_{\mathbf{IR}}$ (dashed) for $\sqrt{s} = 14$ TeV. The left panel shows distribution for c quarks (antiquarks), and the right panel for b quarks (antiquarks) for single-diffractive production.

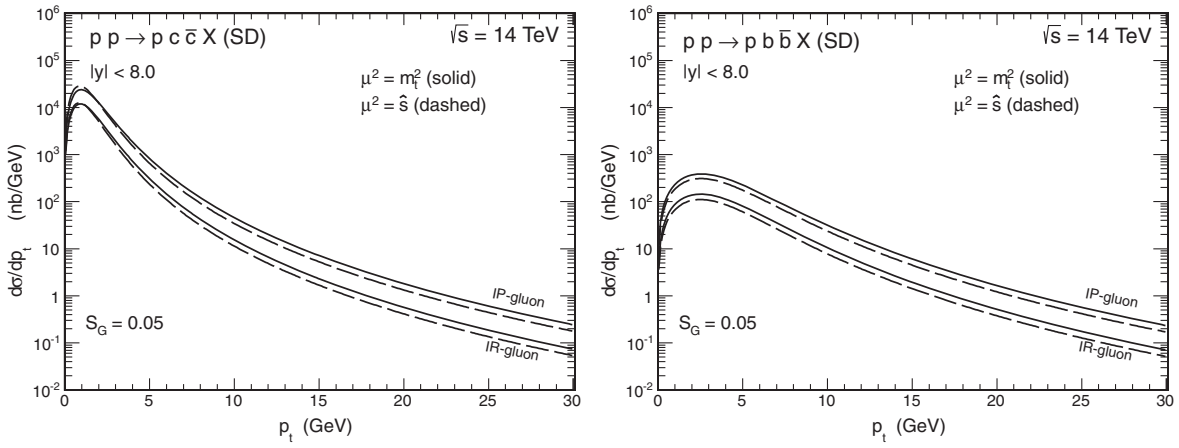

FIG. 8. Transverse momentum distribution of c quarks (antiquarks) (left) and b quarks (antiquarks) (right) for single-diffractive production at $\sqrt{s} = 14$ TeV for factorization scales: $\mu^2 = m_t^2$ (solid) and $\mu^2 = \hat{s}$ (dashed).

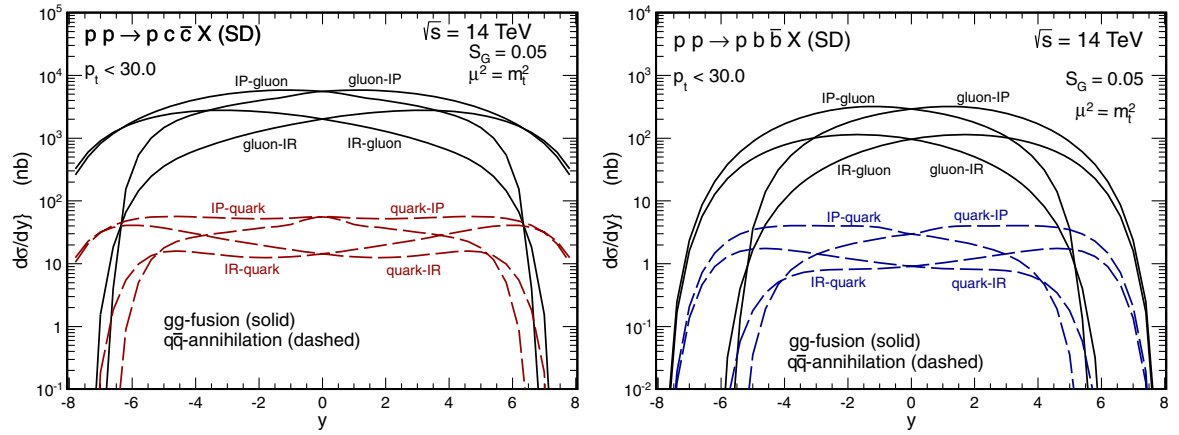

FIG. 9 (color online). Rapidity distribution of c quarks (antiquarks) (left) and b quarks (antiquarks) (right) for single-diffractive production at $\sqrt{s} = 14$ TeV. Components of the Pomeron-gluon (and gluon-Pomeron), the Pomeron-quark/antiquark (and quark/antiquark-Pomeron), the Reggeon-gluon (and gluon-Reggeon), and the Reggeon-quark/antiquark (and quark/antiquark-Reggeon) mechanisms are shown separately.

Figures 9 and 10 show rapidity distributions for c quark (antiquark) (left panels) and b quark (antiquark) (right panels) pair production for single- and central-diffractive mechanisms, respectively. The rapidity distributions for Pomeron-gluon (and gluon-Pomeron), Pomeron-quark/antiquark (and quark/antiquark-Pomeron), and Reggeon-gluon (and gluon-Reggeon), Reggeon-quark/antiquark (and quark/antiquark-Reggeon) mechanisms in the single-diffractive case are shifted to forward and backward rapidities, respectively. The distributions for the individual single-diffractive mechanisms have maxima at large rapidities, while the central-diffractive contribution is concentrated at midrapidities. This is a consequence of limiting integration over $x_{\mathbf{IP}}$ in Eq. (2.5) to $0.0 < x_{\mathbf{IP}} < 0.1$ and over $x_{\mathbf{IR}}$ to $0.0 < x_{\mathbf{IR}} < 0.2$.

Finally, In Fig. 11 we show the missing mass distribution for c quarks (antiquarks) (left panel) and for b quarks (antiquarks) (right panel) for single-diffractive production. Both contributions have similar shapes of distributions. Experimentally, measuring the distributions in invariant mass of D and B mesons would be interesting and will be discussed in the next section.

C. Heavy quark hadronization effects

The transition from quarks and gluons to hadrons, called hadronization or parton fragmentation, can be so far approached only through phenomenological models. In principle, in the case of many-particle final states, the Lund string model [19] and the cluster fragmentation model [20] are usually used, providing good description of the hadronization of the parton system as a whole. However, the hadronization of heavy quarks is usually done with the help of fragmentation functions (FFs) extracted from e^+e^- experiments (see e.g., Refs. [8,21,22]).

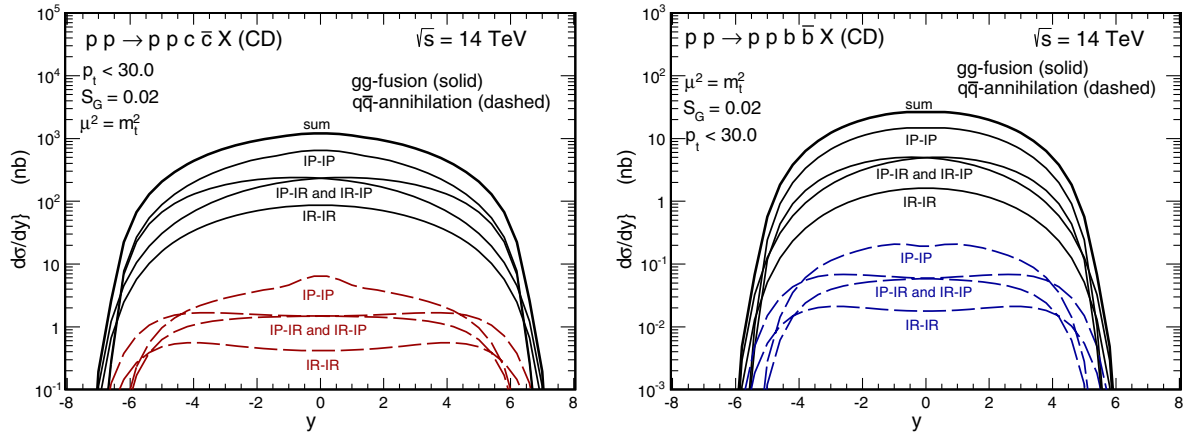

FIG. 10 (color online). Rapidity distribution of c quarks (antiquarks) (left) and b quarks (antiquarks) (right) for the central-diffractive production at $\sqrt{s} = 14$ TeV. Components of the Pomeron-Pomeron, Reggeon-Reggeon, Pomeron-Reggeon and Reggeon-Pomeron mechanisms are shown separately. The sum of all contributions is shown by the thick solid line.

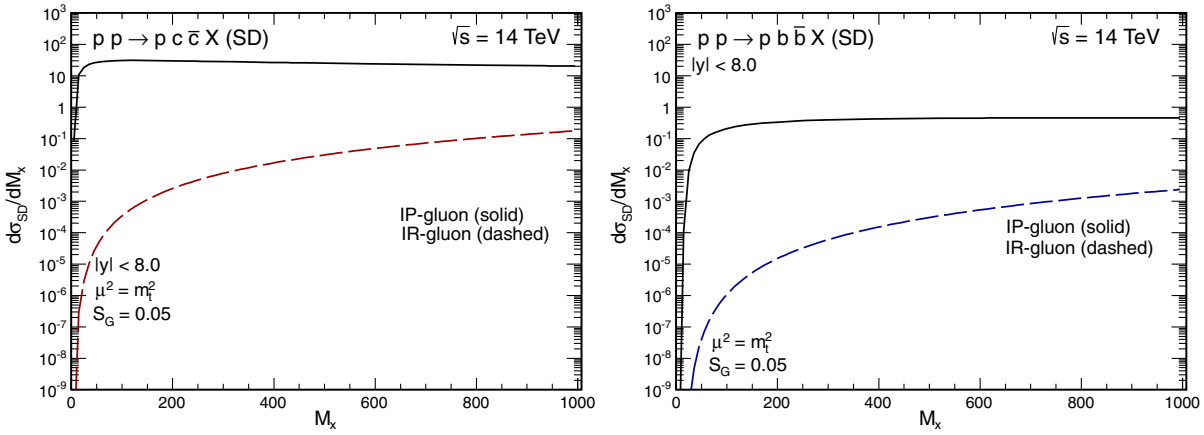

FIG. 11 (color online). The missing mass distribution for $\sqrt{s} = 14$ TeV. The left panel shows the distribution for c quarks (antiquarks), and the right panel for b quarks (antiquarks) for single-diffractive production.

Especially in the case of diffractive production, where one or both protons remain intact, the applicability of the compound hadronization models (implemented in Monte Carlo generators and dedicated to nondiffractive processes) is still an open question. More detailed studies, e.g., of gluonic and quark jet structures in diffractive events, are needed to draw more definite conclusions in this context. In our calculation, we follow the fragmentation function technique which seems to be sufficient to make a first evaluation of corresponding cross sections. This scheme has been recently successfully used for description of inclusive nondiffractive open charm and bottom data at the LHC [8,22]. In the context of diffractive production studies, the uncertainties coming from the process of parton fragmentation seem to be less important than those related to the parton-level diffractive calculation (e.g., uncertainties of diffractive PDFs or gap survival probability).

According to the fragmentation function formalism, in the following numerical calculations, the differential distributions of open charm and bottom hadrons $h = D, B$, e.g., for single-diffractive production, are obtained through a convolution of differential distributions of heavy quarks/antiquarks and $Q \to h$ fragmentation functions:

$$\frac{d\sigma(pp \to h\bar{h}pX)}{dy_h d^2p_{t,h}} \approx \int_0^1 \frac{dz}{z^2} D_{Q\to h}(z) \left.\frac{d\sigma(pp \to Q\bar{Q}pX)}{dy_Q d^2p_{t,Q}}\right|_{\substack{y_Q = y_h \\ p_{t,Q} = p_{t,h}/z}}, \quad (2.7)$$

where $p_{t,Q} = \frac{p_{t,h}}{z}$, and z is the fraction of longitudinal momentum of heavy quark Q carried by a hadron h. Technically, in this scheme of fragmentation, the rescaling of the transverse momentum is the most important effect. This is because one needs to deal with very steep functions of transverse momenta. Since the rapidity spectra are usually flat, or slowly varying, the approximation assuming that y_Q

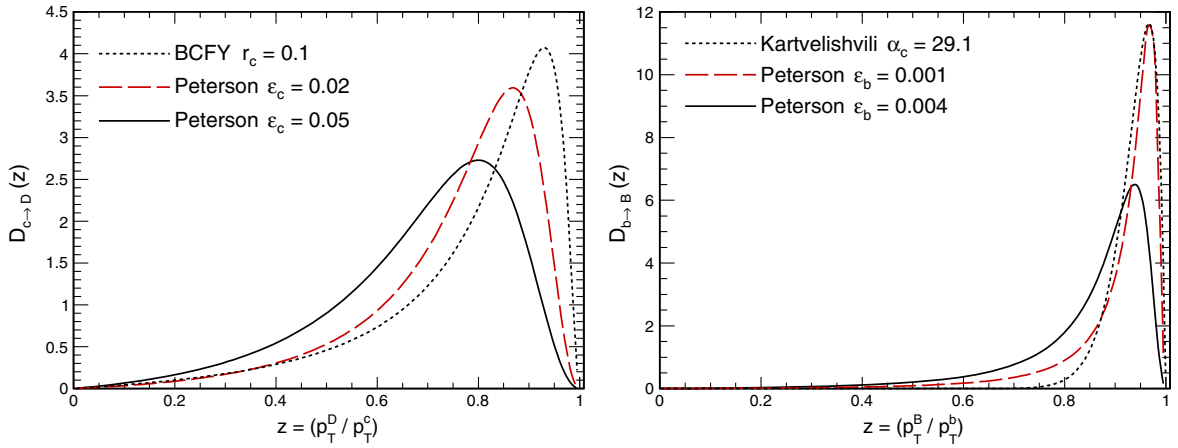

FIG. 12 (color online). Different models of the fragmentation functions for charm (left) and bottom (right) quarks. The default functions from the FONLL framework are compared to the Peterson functions with different ε parameters.

is unchanged in the fragmentation process, i.e., $y_h = y_Q$, is commonly applied. This approximation is typical for light hadrons; however, it is also commonly accepted for heavy quarks, especially in the region of not-too-small quark p_t's. The fragmentation functions for heavy quarks are peaked at large z (see Fig. 12), so the problematic small-p_t region is suppressed.

In all the following numerical calculations, the standard Peterson fragmentation function [23] is applied. The default set of the parameters for these functions is $\varepsilon_c = 0.05$ for charm and $\varepsilon_b = 0.004$ for bottom quarks, respectively. These values were extracted by H1 [24], ALEPH [25], and OPAL [26] analyses. However, in the similar fragmentation scheme applied in the FONLL framework for hadroproduction of heavy flavors at RHIC [21] and LHC [22], rather harder functions are suggested. Within the FONLL approach, the Braaten-Cheung-Fleming-Yuan (BCFY) [27] function with $r_c = 0.1$ for charm and the Kartvelishvili [28] parametrization with $\alpha_b = 29.1$ for bottom are used. In our calculation, to make the shapes of the Peterson functions closer to those from the FONLL approach, the parameters are fixed to $\varepsilon_c = 0.02$ and $\varepsilon_b = 0.001$ (see Fig. 12). In the following numerical predictions of the cross sections for D^0 and $B^\pm$ mesons, the fragmentation functions are normalized to the branching fractions from Refs. [29–31], i.e., $\mathrm{BR}(c \to D^0) = 0.565$ and $\mathrm{BR}(b \to B^\pm) = 0.4$.

D. Cross sections for D^0 and $B^\pm$ meson production

Measurements of charm and bottom cross sections at hadron colliders can be performed in the so-called direct way. This method is based on full reconstruction of all decay products of open charm and bottom mesons, for instance in the $D^0 \to K^-\pi^+$, $D^+ \to K^-\pi^+\pi^+$, or $B^+ \to J/\psi K^+ \to K^+\mu^+\mu^-$ channels. The decay products with an invariant mass from the expected hadron decay combinations permit direct observation of D or B mesons as a peak in the invariant mass spectrum. Then, after a subtraction of the invariant mass continuum, the relevant cross section for

TABLE I. Integrated cross sections for diffractive production of open charm and bottom mesons in different measurement modes for ATLAS, LHCb and CMS experiments at $\sqrt{s} = 14$ TeV.

Acceptance	Mode	Integrated cross sections, [nb]		
		Single-diffractive	Central-diffractive	Nondiffractive EXP data
ATLAS, $\lvert y\rvert < 2.5$ $p_\perp > 3.5$ GeV	$D^0 + \overline{D^0}$	3555.22 (IR: 25%)	177.35 (IR: 43%)	...
LHCb, $2 < y < 4.5$ $p_\perp < 8$ GeV	$D^0 + \overline{D^0}$	31442.8 (IR: 31%)	2526.7 (IR: 50%)	1488000 ± 182000
CMS, $\lvert y\rvert < 2.4$ $p_\perp > 5$ GeV	$(B^+ + B^-)/2$	349.18 (IR: 24%)	14.24 (IR: 42%)	$28100 \pm 2400 \pm 2000$
LHCb, $2 < y < 4.5$ $p_\perp < 40$ GeV	$B^+ + B^-$	867.62 (IR: 27%)	31.03 (IR: 43%)	$41400 \pm 1500 \pm 3100$
LHCb, $2 < y < 4$ $3 < p_\perp < 12$ GeV	$D^0\overline{D^0}$	179.4 (IR: 28%)	7.67 (IR: 45%)	$6230 \pm 120 \pm 230$

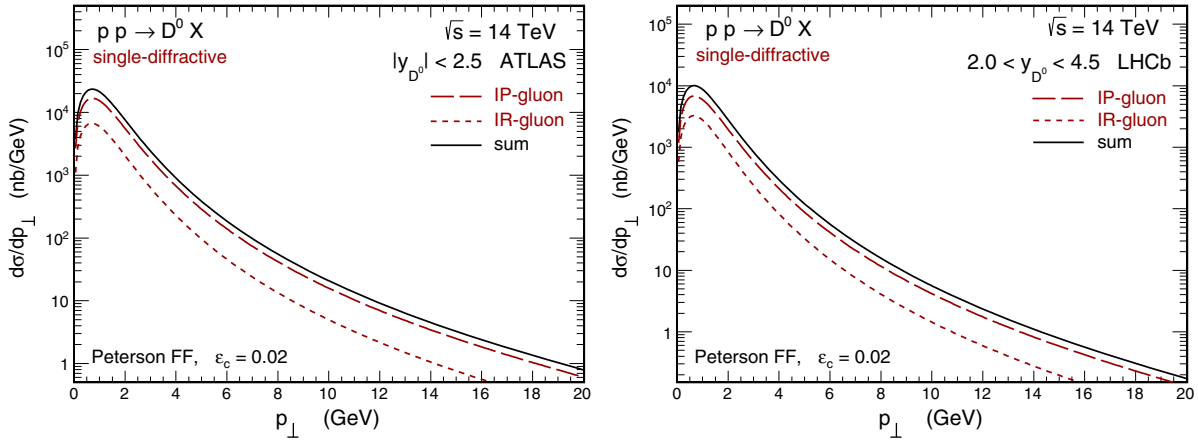

FIG. 13 (color online). Transverse momentum distribution of D^0 meson within the ATLAS (left) and the LHCb (right) acceptance for single-diffractive production at $\sqrt{s} = 14$ TeV. Components of the Pomeron-gluon (and gluon-Pomeron) (long-dashed line) and the Reggeon-gluon (and gluon-Reggeon) (short-dashed line) contributions are shown separately.

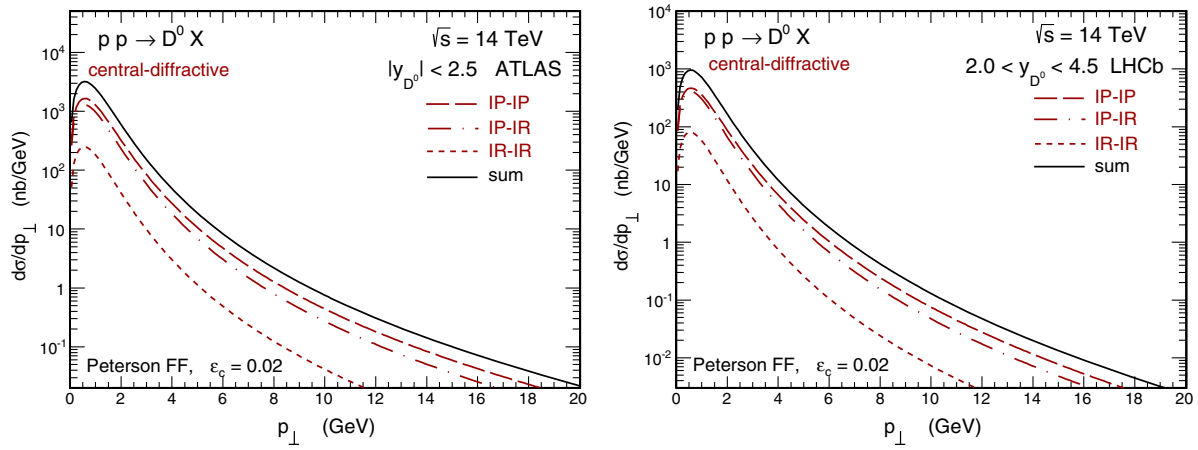

FIG. 14 (color online). Transverse momentum distribution of the D^0 meson within the ATLAS (left) and the LHCb (right) acceptance for central-diffractive production at $\sqrt{s} = 14$ TeV. Components of the Pomeron-Pomeron, Pomeron-Reggeon, Reggeon-Pomeron, and the Reggeon-Reggeon contributions are shown separately.

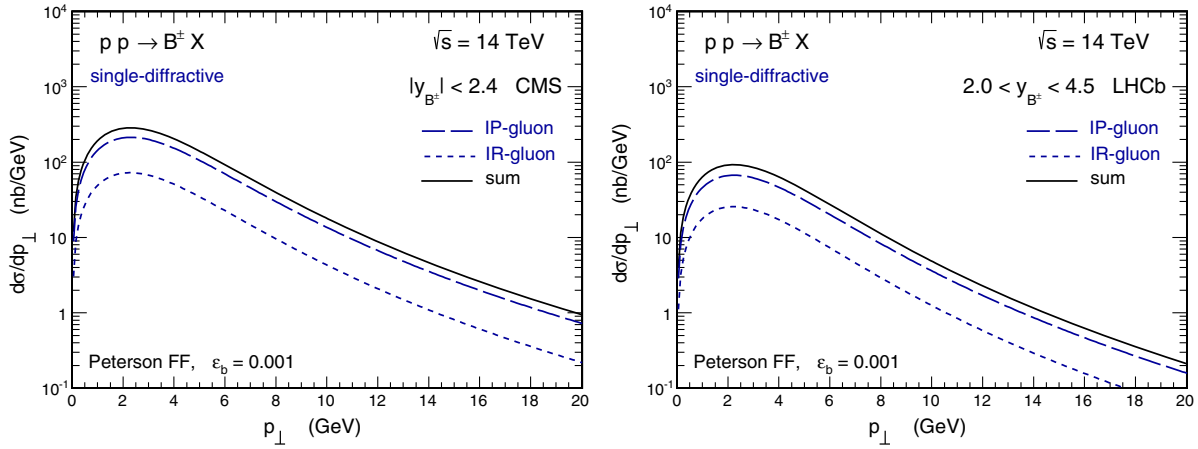

FIG. 15 (color online). Transverse momentum distribution of $B^{\pm}$ mesons within the CMS (left) and the LHCb (right) acceptance for single-diffractive production at $\sqrt{s} = 14$ TeV. Components of the Pomeron-gluon (and gluon-Pomeron) (long-dashed line) and the Reggeon-gluon (and gluon-Reggeon) (short-dashed line) contributions are shown separately.

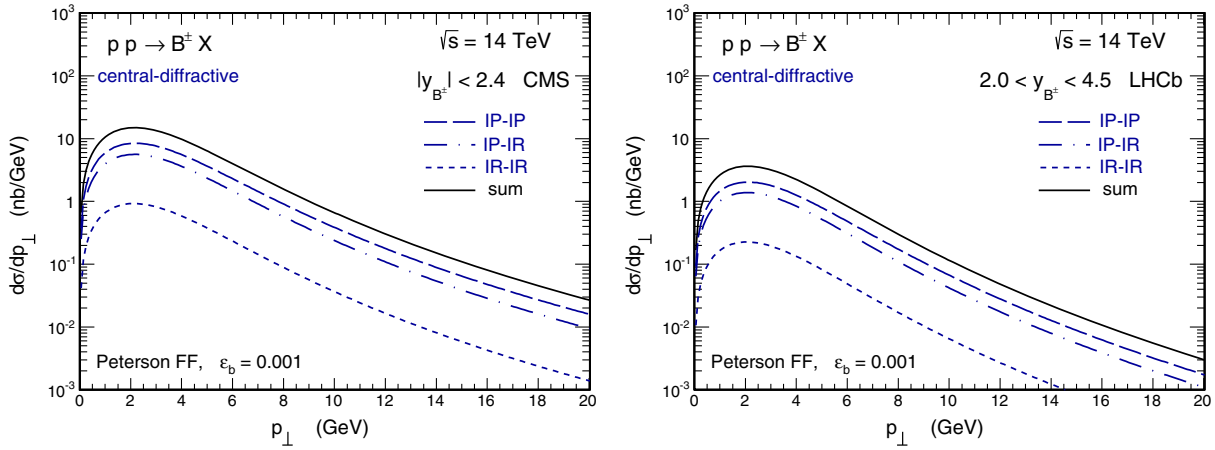

FIG. 16 (color online). Transverse momentum distribution of $B^{\pm}$ mesons within the CMS (left) and the LHCb (right) acceptance for central-diffractive production at $\sqrt{s} = 14$ TeV. Components of the Pomeron-Pomeron, Pomeron-Reggeon, Reggeon-Pomeron, and Reggeon-Reggeon mechanisms are shown separately.

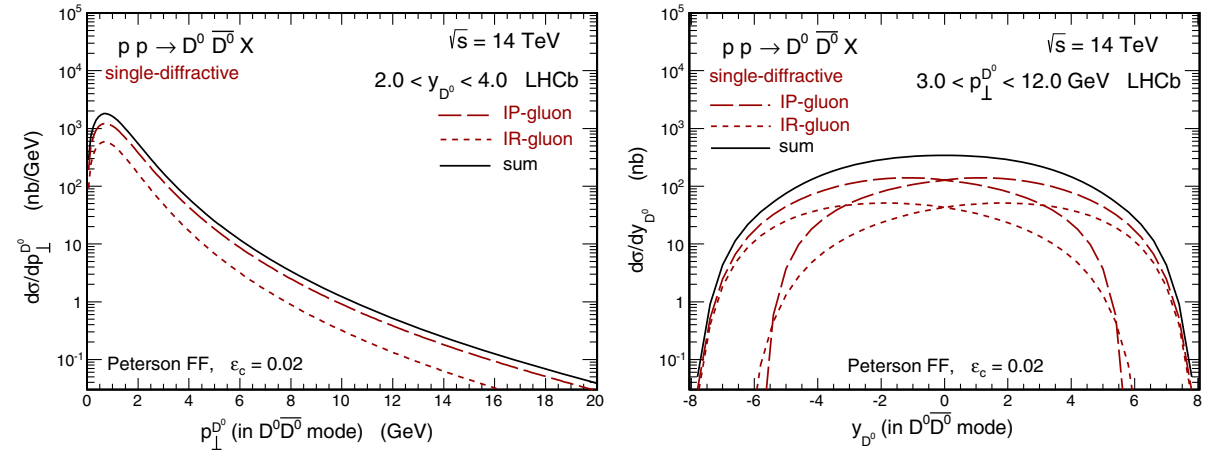

FIG. 17 (color online). Transverse momentum (left) and rapidity (right) distributions of the D^0 meson within the LHCb acceptance provided that $\overline{D^0}$ was registered too, for the single-diffractive mechanisms at $\sqrt{s} = 14$ TeV. Components of the Pomeron-gluon (and gluon-Pomeron) (long-dashed line) and the Reggeon-gluon (and gluon-Reggeon) (short-dashed line) contributions are shown separately.

the meson production can be provided. The same method can be applied for measurement of charm and bottom production rates for the diffractive events.

Numerical predictions of the integrated cross sections for the single- and central-diffractive production of D^0 and $B^{\pm}$ mesons, including relevant experimental acceptance of the ATLAS, LHCb, and CMS detectors, are collected in Table I. The kinematical cuts are taken to be identical to those which have been already used in the standard nondiffractive measurements of open charm and bottom production rates at the LHC. The corresponding experimental cross sections for nondiffractive processes are shown for reference. In the case of inclusive production of single D or B mesons, the ratio of the diffractive integrated cross sections to the nondiffractive one is about ~2% for single- and only about ~0.07% for central-diffractive mechanism. This ratio is only slightly bigger for $D^0\overline{D^0}$ pair production, becoming about ~3% and 0.1%, respectively. In addition, the relative contribution of the Reggeon exchange mechanisms to the overall diffractive production cross sections is shown. This relative contribution is about ~24%–31% for single-diffractive ($\frac{\mathrm{IR}}{\mathrm{IP+IR}}$) and ~42%–50% for central-diffractive processes ($\frac{\mathrm{IPIR+IRIP+IRIR}}{\mathrm{IPIP+IPIR+IRIP+IRIR}}$) for both charm and bottom flavored mesons. The ratio does not really change for different measurement modes and different experimental acceptance.

Figures 13 and 14 show transverse momentum distributions of D^0 meson at $\sqrt{s} = 14$ TeV within the ATLAS (left panels) and the LHCb (right panels) acceptance for single- and central-diffractive production, respectively. The contributions of the Pomeron (long-dashed lines) and Reggeon exchange (short-dashed lines) mechanisms are shown

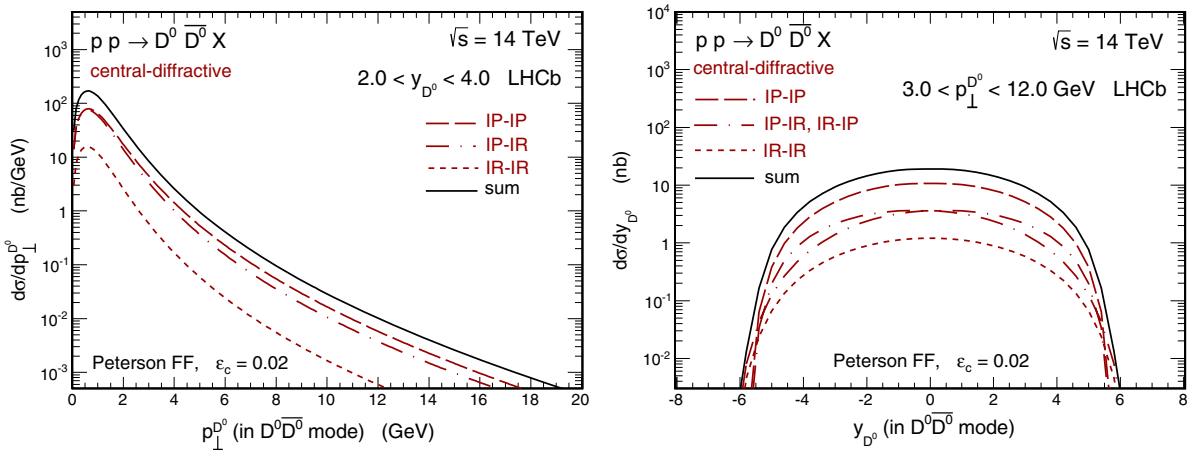

FIG. 18 (color online). Transverse momentum (left) and rapidity (right) distributions of the D^0 meson within the LHCb acceptance provided that $\overline{D^0}$ was registered too, for the central-diffractive mechanism at $\sqrt{s} = 14$ TeV. Components of the Pomeron-Pomeron, Pomeron-Reggeon, Reggeon-Pomeron and Reggeon-Reggeon contributions are shown separately.

separately. These two contributions have similar shapes of the distributions and differ only in normalization. Therefore, one should not expect a possibility to extract and to test the Reggeon component within the special cuts in transverse momentum. The similar distributions (with identical conclusions) but for $B^{\pm}$ mesons within the CMS (left panels) and the LHCb (right panels) acceptance are presented in Figs. 15 and 16.

Figures 17 and 18 show transverse momentum (left panels) and rapidity (right panels) distributions of the D^0

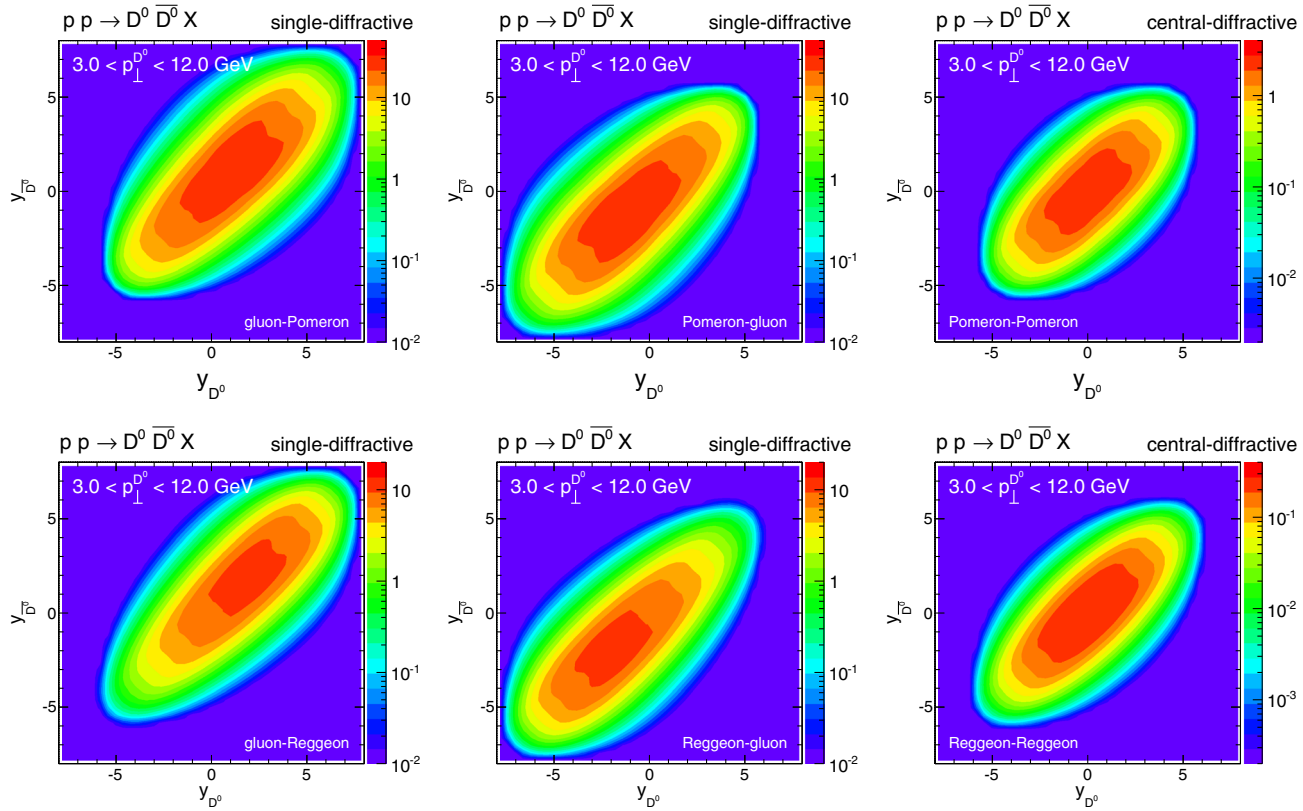

FIG. 19 (color online). Double differential cross sections as a function of D^0 and $\overline{D^0}$ rapidities within the LHCb detector acceptance for single- (left and middle panels) and central-diffractive (right panels) production at $\sqrt{s} = 14$ TeV. The top and bottom panels correspond to the Pomeron and Reggeon exchange mechanisms, respectively.

(or $\overline{D^0}$) meson at $\sqrt{s} = 14$ TeV within the LHCb acceptance in the case of $D^0\overline{D^0}$ pair production for single- and central-diffractive mechanisms, respectively. The graphical representation of Pomeron and Reggeon exchange contributions is the same as in the previous figures. The rapidity distributions for Pomeron-gluon (or Reggeon-gluon) and gluon-Pomeron (or gluon-Reggeon) mechanisms in the single-diffractive case are shifted to forward and backward rapidities, respectively. Since the rapidity acceptance of the LHCb detector is not symmetric in rapidity and covers only forward region $2 < y_{D^0} < 4$, each of these single-diffractive mechanisms contributes to the $D^0\overline{D^0}$ pair diffractive cross section in a quite different way. The situation is shown in more detail in Fig. 19, where the rapidity correlations between D^0 and $\overline{D^0}$ meson are depicted. In all the considered cases, these distributions show some correlation along the diagonal. Clearly some shifts of the distributions for the single-diffractive mechanism can be seen, in contrast to the central-diffractive one.

III. CONCLUSIONS

Although there was a lot of theoretical activity in calculating diffractive production of different objects [gauge bosons (W, Z), jets or dijets, Higgs bosons, pairs of gauge bosons (W^+W^-)] in proton-proton or proton-antiproton collisions, almost no detailed experimental studies were performed and presented in the literature. Such a study would be interesting and important in order to understand the mechanism of diffractive production. This is partly so, as many reactions considered so far have very small cross sections. So far, there is no common agreement on what is the underlying mechanism of diffractive production. Since the underlying dynamics is of nonperturbative nature, any detailed studies would therefore be very helpful to shed new light on the problem.

In the present paper, we discuss in more detail single- and central-diffractive production of charm and bottom quark-antiquark pairs as well as open charmed and bottom mesons. The corresponding cross sections are rather large.

In the present study, we have limited ourselves to the most popular Ingelman-Schlein model of resolved Pomerons and Reggeons. Although there is no experimental proof for the model and its underlying dynamics, it has the advantage of having been used to describe many diffractive processes at HERA. In the purely hadronic processes considered in the present paper, it must be supplemented by including absorption effects due to nonperturbative interaction of hadrons (protons).

In our approach, we use diffractive parton distribution in the proton obtained at HERA from the analysis of the diffractive structure function of the proton and the diffractive production of jets. Both Pomeron and Reggeon contributions are considered here.

First, we have calculated cross sections for $c\bar{c}$ and $b\bar{b}$ production in single and central production. Several quark-level differential distributions are shown and discussed. We have compared Pomeron and Reggeon contributions for the first time.

In order to make predictions which could be compared with future experimental data, in the next step we have included hadronization to charmed (D) and bottom (B) mesons using a practical method of hadronization functions known for other processes. We have shown several inclusive differential distributions for the mesons as well as correlations of D and $\bar{D}$ mesons. In these calculations we have included detector acceptance of the ATLAS, CMS, and LHCb collaboration experiments.

The production of charmed mesons is extremely interesting because of the cross section of the order of a few microbarns for ATLAS and CMS and of the order of tens of microbarns for the LHCb acceptance. We have shown that the Pomeron contribution is much larger than the subleading Reggeon contribution. Especially, the LHCb main detector supplemented with VELO (VErtex LOcator) micro-strip silicon detectors installed already in run I and the so-called HERSCHEL (High Rapidity Shower Counters for LHCb) apparatus to be installed in run II could be used to measure D mesons (main detector) and define the rapidity gap necessary for diffractive production (VELO and/or HERSCHEL). On the other hand, the ATLAS and CMS collaboration could use ALFA and TOTEM detectors to measure forward protons. Then different additional differential distributions are possible.

ACKNOWLEDGMENTS

We are indebted to Guy Wilkinson from the LHCb Collaboration for discussion of the LHCb possibilities and Wolfgang Schäfer for several interesting discussions of diffractive processes and heavy quark production in particular. We wish to thank Rafał Staszewski and Maciej Trzebiński for continued interest in our studies. This work was partially supported by the Polish NCN Grant No. DEC-2013/09/D/ST2/03724.

[1] G. Ingelman and P. E. Schlein, Phys. Lett. **152B**, 256 (1985).
[2] M. Klasen and G. Kramer, Phys. Rev. D **80**, 074006 (2009).
[3] L. Alvero, J. C. Collins, J. Terron, and J. J. Whitmore, Phys. Rev. D **59**, 074022 (1999).
[4] A. Cisek, W. Schäfer, and A. Szczurek, Phys. Rev. D **80**, 074013 (2009).
[5] M. Łuszczak, A. Szczurek, and Ch. Royon, J. High Energy Phys. 02 (2015) 098.
[6] M. Łuszczak, R. Maciuła, and A. Szczurek, Phys. Rev. D **84**, 114018 (2011).
[7] C. Marquet, C. Royon, M. Trzebiński, and R. Zlebcik, Phys. Rev. D **87**,034010 (2013).
[8] R. Maciula and A. Szczurek, Phys. Rev. D **87**, 094022 (2013).
[9] A. Aktas *et al.* (H1 Collaboration), Eur. Phys. J. C **48**, 715 (2006).
[10] A. D. Martin, W. J. Stirling, R. S. Thorne, and G. Watt, Eur. Phys. J. C **64**, 653 (2009).
[11] A. Szczurek, N. N. Nikolaev, and J. Speth, Phys. Lett. B **428**, 383 (1998).
[12] A. Aktas *et al.* (H1 Collaboration), Eur. Phys. J. C **48**, 749 (2006).
[13] S. Chekanov *et al.* (ZEUS Collaboration), J. High Energy Phys. 06 (2009) 074.
[14] S. Donnachie, H. G. Dosch, O. Nachtmann, and P. Landshoff, Cambridge Monogr. Part. Phys., Nucl. Phys., Cosmol. **19**, 1 (2002).
[15] P. Lebiedowicz and A. Szczurek, Phys. Rev. D **81**, 036003 (2010); P. Lebiedowicz, R. Pasechnik, and A. Szczurek, Phys. Lett. B **701**, 434 (2011).
[16] V. A. Khoze, A. D. Martin, and M. G. Ryskin, Eur. Phys. J. C **18**, 167 (2000).
[17] U. Maor, AIP Conf. Proc. **1105**, 248 (2009).
[18] W. Schafer and A. Szczurek, Phys. Rev. D **76**, 094014 (2007).
[19] B. Andersson, G. Gustafson, G. Ingelman, and T. Sjostrand, Phys. Rep. **97**, 31 (1983).
[20] B. R. Webber, Nucl. Phys. **B238**, 492 (1984).
[21] M. Cacciari, P. Nason, and R. Vogt, Phys. Rev. Lett. **95**, 122001 (2005).
[22] M. Cacciari, S. Frixione, N. Houdeau, M. L. Mangano, P. Nason, and G. Ridolfi, J. High Energy Phys. 10 (2012) 137.
[23] C. Peterson, D. Schlatter, I. Schmitt, and P. M. Zerwas, Phys. Rev. D **27**, 105 (1983).
[24] F. D. Aaron *et al.* (H1 Collaboration), Eur. Phys. J. C **59**, 589 (2009).
[25] A. Heister *et al.* (ALEPH Collaboration), Phys. Lett. B **512**, 30 (2001).
[26] G. Abbiendi *et al.* (OPAL Collaboration), Eur. Phys. J. C **29**, 463 (2003).
[27] E. Braaten, K.-m. Cheung, S. Fleming, and T. C. Yuan, Phys. Rev. D **51**, 4819 (1995).
[28] V. G. Kartvelishvili, A. K. Likhoded, and V. A. Petrov, Phys. Lett. **78B**, 615 (1978).
[29] E. Lohrmann, arXiv:1112.3757.
[30] J. Beringer *et al.* (Particle Data Group), Phys. Rev. D **86**, 010001 (2012).
[31] T. Aaltonen *et al.* (CDF Collaboration), Phys. Rev. D **77**, 072003 (2008).